



HAL
open science

Vibrational Response of Au-Ag alloy and Porous Au Single nanowires Probed by Ultrafast Pump-Probe Spectroscopy

R Delalande, L Burr, E. Charron, M Jouini, M E Toimil-Molares, L Belliard

► **To cite this version:**

R Delalande, L Burr, E. Charron, M Jouini, M E Toimil-Molares, et al.. Vibrational Response of Au-Ag alloy and Porous Au Single nanowires Probed by Ultrafast Pump-Probe Spectroscopy. 2019. hal-02134035v1

HAL Id: hal-02134035

<https://hal.science/hal-02134035v1>

Preprint submitted on 29 May 2019 (v1), last revised 23 Sep 2020 (v2)

HAL is a multi-disciplinary open access archive for the deposit and dissemination of scientific research documents, whether they are published or not. The documents may come from teaching and research institutions in France or abroad, or from public or private research centers.

L'archive ouverte pluridisciplinaire **HAL**, est destinée au dépôt et à la diffusion de documents scientifiques de niveau recherche, publiés ou non, émanant des établissements d'enseignement et de recherche français ou étrangers, des laboratoires publics ou privés.

Vibrational Response of Au-Ag alloy and Porous Au Single nanowires Probed by Ultrafast Pump-Probe Spectroscopy

R. Delalande,¹ L. Burr,² E. Charron,¹ M. Jouini,¹ M. E. Toimil-Molares,² and L. Belliard^{1, a)}

¹⁾*Institut des NanoSciences de Paris, Sorbonne Université, UPMC Universités Paris 06, UMR 7588, Paris F-75005, France*

²⁾*Materials Research Department, GSI Helmholtz Centre for Heavy Ion Research, Planckstr. 1, 64291 Darmstadt Germany*

We report on ultrafast vibrational response of single Au-Ag alloy and Au porous nanowires obtained by the template method. The oscillations of the sample reflectivity are correlated to eigenmodes (EM) confined in the nanowire. Taking advantage of a free standing geometry, we are able to detect few harmonics. Coupling electron microscopy and pump-probe investigations with very high spectral resolution performed on the same wire, we demonstrate that both longitudinal and transverse sound velocity could be obtained for variable Au concentration. Additional quadrupolar mode is also observed and reproduced by finite element simulation. Finally, porous nanowire are investigated.

Keywords: Nanowires, Au-Ag Alloy nanowire, Porous Au nanowire, Pump-probe Spectroscopy, Vibrations

In the past few decades, multicomponent heterostructure nanowires (NW) have received a great interest from the fundamental as well as from the application point of view. This interest originates from the fact that specific functionalities are expected when several materials are purposely combined in the same single nanostructure^{1,2}. Different types of heterostructures such as core-shell, multilayered, alloy or nanoporous NWs are being developed and characterized, and find applications in fields such as magnetism³⁻⁵, catalysis^{6,7}, electronics⁸⁻¹⁰, optics¹¹⁻¹⁵, biological sensing¹⁶, fuel cells¹⁷, solar energy harvesting¹⁸⁻²⁰, microactuators²¹ or acoustics^{22,23}.

The impact of size reduction down to the nanoscale also attracts considerable attention especially on acoustic responses. Indeed, confinement deeply modifies the acoustic dispersion relations compared with the bulk counterparts. This, in turn, strongly influences the thermal^{24,25} and electronic²⁶ properties of the nanostructures, characteristics which must be carefully taken into consideration during the development of NW based devices, such as thermoelectric, photonic, or electronic devices^{25,27-29}.

The Young's modulus of nanostructures has been determined using various techniques, such as atomic force microscopy³⁰, transmission electron microscopy³¹, or, alternatively, time-resolved pump and probe spectroscopy where an ultra-short femtosecond pump pulse induces a fast heating³². The excited EM of the nano-object are subsequently optically detected by a time-delayed probe pulse. This pump-probe method is nowadays considered a very powerful tool to address local elasticity issues into nanostructures, particularly interesting for being contact-less and for not requiring special sample preparation.

Since the pioneer work of van Dijk³³, who investigated the dynamic response of single gold nanospheres, a large number of materials and nanoobject shapes has been investigated³⁴⁻⁴⁰. In the special case of infinite long

NWs the major literature deals with semiconductor material⁴¹⁻⁴³ or pure metallic material⁴⁴⁻⁴⁹.

In this letter we report on the dynamic response of single Au-Ag alloy NW with diameter around 200 nm, length of few μm , and a controlled gold molar fraction of 30, 40, and 60%. In addition, the Ag is selectively dealloyed from the NW, and the properties of the resulting porous Au NW are also examined. In order to improve the measurements, individual NW are transferred onto pre-structured substrates with μm -wide trenches. Indeed, when a NW rest free-standing on a cavity or trench the energy relaxation channel through the substrate is suppressed and the NW nanoresonators exhibit higher quality factors⁴⁶. Applying this geometry, breathing harmonics and quadrupole mode response have been observed. The standard Pochhammer-Chree model coupled with scanning electron microscopy (SEM) measurements are combined to successfully obtain a complete characterization of the longitudinal and transverse sound velocities in the Au-Ag NWs for each Au concentrations. Finite element simulations are also performed in order to complete our investigation and interpretations.

The NWs were synthesized by electrodeposition in etched ion-track membranes. First, 30 μm thick polycarbonate foils (Makrofol N, Bayer AG) were irradiated with 2 GeV Au ions at the UNILAC linear accelerator of GSI Helmholtz Centre (Darmstadt, Germany). Prior to etching, each side of the foils is exposed to UV light for one hour. The ion-tracks created by ions are subsequently selectively dissolved in a 2M NaOH solution at 50°C for 30 min, resulting in cylindrical nanochannels with average diameter 200 nm. After etching, a thick Au layer is sputtered on one side of the polymer membrane, and reinforced with an electrodeposited Au layer (thickness few μm). This layer acts as a working electrode during the deposition of Au and Au-Ag inside the nanochannels. Details of the electrodeposition of Au and Au-Ag alloy NWs have been previously published⁵⁰. The polymer membrane is then removed by immersing the sample in several baths of dichloromethane solution and the NWs are detached from the Au electrode by a short

^{a)}Electronic mail: laurent.belliard@upmc.fr

sonication on clean dichloromethane. Finally, individual Au-Ag NWs are pipetted onto the pre-structured Si substrates. The process is optimized such that enough NWs are free-standing between two adjacent beams. To produce porous Au wires, the substrate with the Au-Ag NWs is immersed in a nitric acid solution for 3 hours, rinsed with 3 subsequent MilliQ water baths and dried in air.

The experimental setup used during this study working in reflection geometry in an inverse Olympus microscope has been described in detail in previous works^{51,52}. Ultrafast pump-probe spectroscopy experiments are performed using a mode-locked Ti:sapphire (MAI-TAI Spectra) laser source operating at 800 nm with a pulse duration below 100 fs at the laser output and a repetition rate of 78.8 MHz. Synchronous detection on the sample reflectivity is performed by modulating the pump beam at 1.8 MHz. Both pump and probe beams are focused by means of a microscope objective with a NA= 0.9 and are normally incident on the sample. The laser spots can be focused around 1 μm diameter at $1/e^2$. A two-color experiment is performed by doubling the pump frequency (400 nm) with a nonlinear crystal (Beta barium borate or BBO) to avoid scattered light coming from the pump beam. A dichroic filter located in front of the diode system suppresses the light of the pump beam, its power on the sample is reduced around 300 μW , and the power of the probe beam does not exceed 50 μW to prevent from any damage. Such conditions guarantee that the experiments are performed in the thermoelastic regime and that both acoustic signal and optical reflectivity remain stable during all the average processing. The sample reflectivity is measured by an avalanche photodiode and analyzed with a lock-in amplifier. A maximum pump-probe time delay equal to 12 ns is achieved using a mobile reflector system mounted on a translation stage.

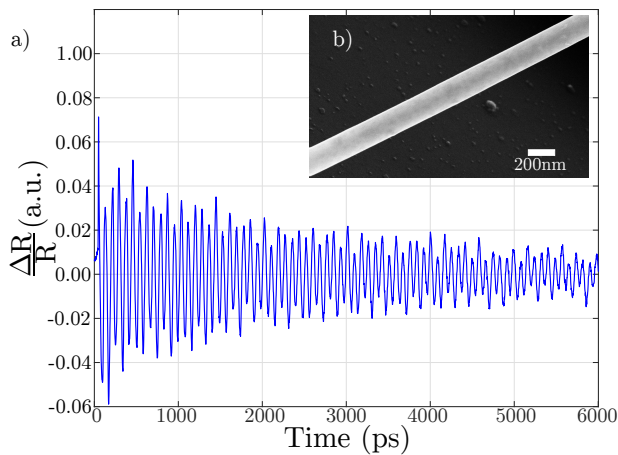


FIG. 1: a) Time resolved reflectivity response measured on a single 200 nm diameter Au nanowire placed across a trench. b) Scanning electron microscopy image of a single Au nanowire.

Figure 1 a) presents the oscillations of reflectivity $\frac{\Delta R}{R}$ measured on a 200 nm diameter single Au NW above a trench. A SEM image of this NW is shown in figure 1

b). The subsequent frequency analysis of the reflectivity signal is shown on figure 2. It evidences a main frequency component around $f_2 = 12.2$ GHz as well as several other components at $f_3 = 29.3$ and $f_4 = 46.3$ GHz and a low-frequency component around $f_1 = 5.0$ GHz.

Those components reveal the vibrations of the Au NW. In particular, the components numbered as f_2 , f_3 , and f_4 correspond to the first three breathing modes (BM) of the wire exhibiting pure radial displacement. This is found by solving the Navier equation in an infinite isotropic NW in order to obtain the Pochhammer-Chree equation^{53,54} which can be approximated for such a mode in the long wavelength assumption under the form

$$2 \frac{v_T}{v_L} J_1 \left(\frac{\omega_n a}{v_L} \right) - \frac{\omega_n a}{v_T} J_0 \left(\frac{\omega_n a}{v_L} \right) = 0, \quad (1)$$

where a is the wire radius, J_0 and J_1 correspond to the Bessel function of the zeroth and first kind, respectively, $\omega_n = 2\pi f_n$ is the pulsation of mode n , and v_L and v_T are the longitudinal and transverse sound velocities.

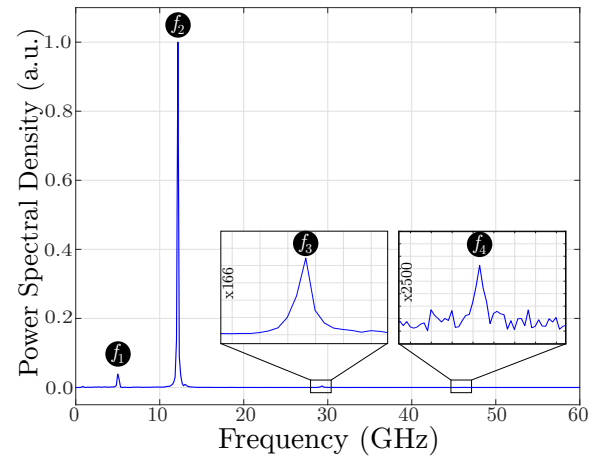


FIG. 2: Normalized power spectral density of the signal shown on figure 1 presenting 3 frequency components at $f_2 = 12.1$, $f_3 = 29.3$ and $f_4 = 46.3$ GHz assigned to radial breathing modes as well as a lower signature at $f_1 = 5.0$ GHz related to a quadrupolar mode geometry. Those components presents respectively quality factor of $Q_1 = 16$, $Q_2 = 67$, $Q_3 = 107$ and $Q_4 = 76$.

However, even if the frequencies of these 3 modes are known, the three unknown parameters a , v_L , and v_T can't yet be unambiguously determined due to the mathematical structure of the equation 1. This is circumvented by determining the radius of the excited NW, a , by SEM. For this, after the pump-probe measurements the same NW was located under the SEM beam using the numbered marks on the trenches.

Subsequently, the (v_L, v_T) couples solutions of equation 1 were determined for each frequency for the measured value of a . Figure 3 shows the transverse velocities, plotted as function of the longitudinal ones, for f_2 (blue dotted line), f_3 (green continuous line), and f_4 (red dashed line). Three different curved lines are obtained. As these three frequency components are simultaneously

Materials	E (GPa)	γ	ρ ($\text{kg}\cdot\text{m}^{-3}$)
Au	78	0.43	$1.93 \cdot 10^4$
Ag	84	0.37	$1.05 \cdot 10^4$

TABLE I: Values of the Young's Modulus E , the Poisson's ratios γ and the densities ρ of gold and silver.

observed on the spectrum, the unique possible (v_L , v_T) couple is obtained by the intersection point.

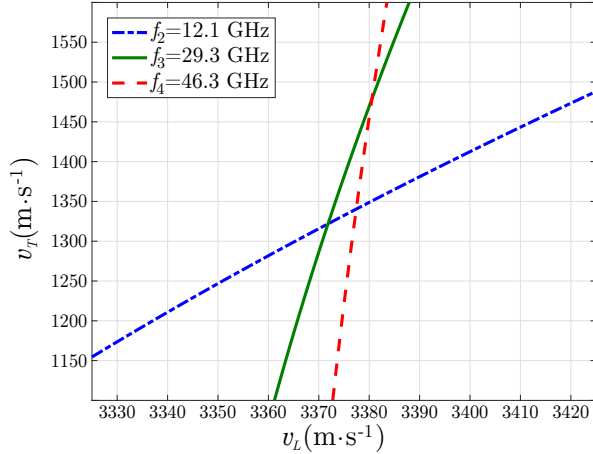


FIG. 3: Couples of longitudinal and transverse velocities solutions of the equation 1 for the first three breathing mode frequency for $a = 200.1$ nm.

The slope of these curves increases with the harmonic order, indicating that the resonance frequency is less and less sensitive to the transverse velocity as it has been previously demonstrated³². As shown on figure 3, a single intersection point is not obtained but instead three intersection points quite close to each other. It leads to the average values $v_L^M = 3378$ $\text{m}\cdot\text{s}^{-1}$ and $v_T^M = 1381$ $\text{m}\cdot\text{s}^{-1}$ as well as the standard deviations $\sigma_{v_L} = 4$ $\text{m}\cdot\text{s}^{-1}$ and $\sigma_{v_T} = 86$ $\text{m}\cdot\text{s}^{-1}$. We'd like to emphasize that the relative standard deviations obtained in this way are 0.12% and 6.2% for the longitudinal and transverse velocity respectively.

To investigate how velocities vary as a function of the NW composition, several NWs with nominal diameter but different molar fractions of gold and silver (namely $\text{Au}_{0.3}\text{Ag}_{0.7}$, $\text{Au}_{0.4}\text{Ag}_{0.6}$ and $\text{Au}_{0.6}\text{Ag}_{0.4}$) were characterized in the same manner as described above. However, in the case of alloy wires the analysis was based on only 2 frequency components, since only two BM were recorded in most of the cases. Simultaneously, two homogenization models are used to calculate both velocities from the Young's modulus, Poisson's ratio, and density of bulk gold and silver properties given in table I. The obtained results are plotted in figure 4 together with the experimental values.

As shown on figure 4, both transverse and longitudinal velocities obtained experimentally increase as the gold molar fraction decrease. This tendency is coherent with the prediction made from the Voigt and Reuss

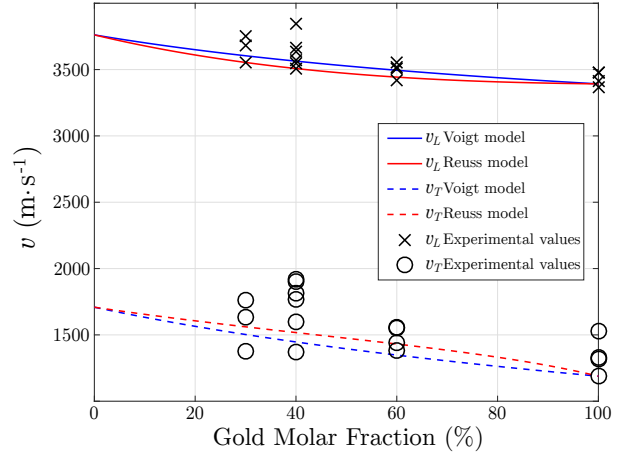


FIG. 4: Transverse and longitudinal velocities obtained experimentally compared to those obtained thanks to Voigt and Reuss models.

models. Nevertheless, one can notice that the relative dispersion of the experimental values from the models is more important for the transverse than for the longitudinal velocity. This is a consequence of the BM being less sensitive to the former than to the latter. A more important scattering of the experimental values for lower gold molar fraction is distinguishable for both velocities. SEM investigations reveal an increase in surface roughness, or the presence of particles on the surface of NWs with higher Ag, figure 5 a), concentration, whereas the Au NWs are smooth, figure 5 b). Moreover, it has been highlighted a surface enrichment of the main metal for such alloys meaning that a Ag-rich layer in $\text{Au}_{0.4}\text{Ag}_{0.6}$ wires and a Au-rich layer in $\text{Au}_{0.6}\text{Ag}_{0.4}$ wires can be observed⁵⁰. Those phenomena could cause a change of the BM frequencies that could explain the scattering of values observed for higher silver molar fraction.

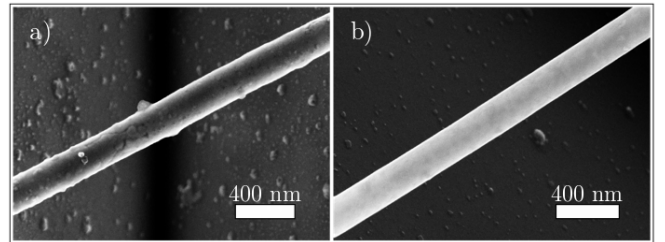


FIG. 5: a) Scanning electron microscopy (SEM) image of a $\text{Au}_{0.3}\text{Ag}_{0.7}$ NW. b) SEM image of a $\text{Au}_{1.0}$ NW.

The first component of the spectrum shown on figure 2, i.e. f_1 , can also be used in order to determine the mechanical properties of the NW. The velocities obtained experimentally by the BM method lead, with the density of bulk Au, to the experimental values for both Young's modulus $E_{exp} = 90.8 \pm 8.1$ GPa and Poisson's ratio $\nu_{exp} = 0.41 \pm 0.01$ which happened to be slightly different from the Au bulk. Those mechanical parameters can then be used to run finite element simulations using the Comsol software to estimate non pure isotropic

radial EM. Among such modes, a quadrupolar mode can be identified at 4.94 GHz, very close to the experimental value of f_1 shown on figure 2. Figure 6 b) represents its mode shape. A relative error on the frequency less than 4% may be deduced from measurements performed on multiple NW, proof that the estimations of both velocities are coherent. Photonic EM exhibiting such angular symmetry have been recently reported in Si NW⁵⁵ and may be assigned to the quadrupolar phonon mode excitation. Naturally the efficiency of such mechanism is much lower than the uniform heat excitation which is at the origin of the BM generation.

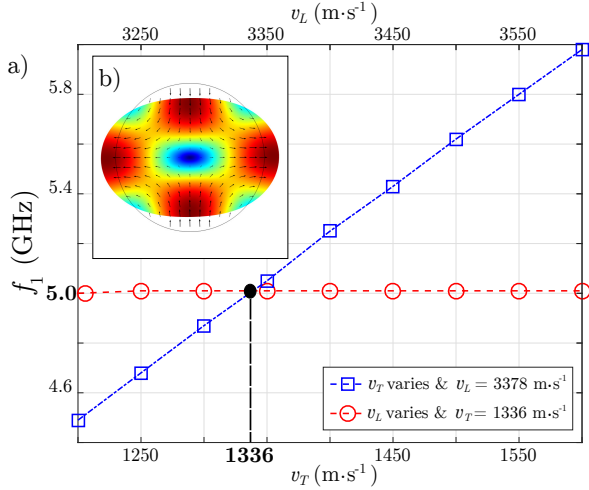


FIG. 6: a) Variation of f_1 for a given value of v_L and varying v_T (blue) and for a given value of v_T and varying v_L (red). b) Mode shape calculated by finite element simulation.

The sensitivity of this quadrupolar mode to both longitudinal and transverse velocities can be investigated by running finite element simulations for different velocity couples and extracting the frequency of the mode. The obtained results for different values of v_L while v_T is fixed, and vice versa, represented on figure 6 indicate that this mode is more sensitive to the transverse than to the longitudinal velocity.

It is proposed to use the value of f_1 measured experimentally as well as the value of v_L obtained by the BM method in order to determine a more accurate value of v_T . Using this method and some finite element simulations, one can improve the estimation of v_T from 1381 ± 86 m.s⁻¹ obtained from figure 3 to 1336 ± 22 m.s⁻¹.

As shown on figure 6, when the fixed value of v_L used is the one given by the BM method and the fixed value of v_T is the one obtained by this second method, the intersection point of those two curves has for ordinate the value of f_1 obtained experimentally. Knowing f_1 and v_L , the accurate value of v_T can then be obtained graphically.

This added process allow one to obtain a more accurate value of the transverse velocity in addition to the accurate value for the longitudinal velocity from the BM method. Nevertheless, it requires to measure the frequency of the quadrupolar mode which is not the case for every NW.

Results obtained on Au_{0.4}Ag_{0.6} NWs before and after

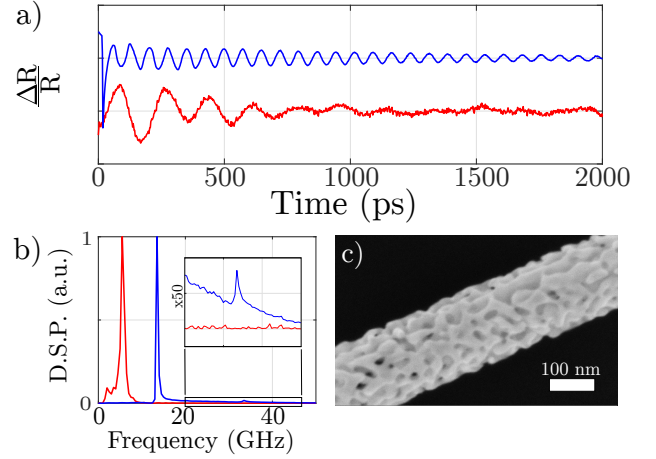


FIG. 7: a) Time resolved reflectivity response measured on a single Au_{0.4}Ag_{0.6} alloy nanowire (blue) and a Au porous nanowire with a porosity of $\phi = 0.6$ (red). b) Corresponding power spectral density showing $f_2 = 13.5$ GHz and $Q_2 = 24$ for the alloy and $f_2 = 5.5$ GHz and $Q_2 = 6$ for the porous c) Scanning electron microscopy image of the porous nanowire.

dealloying were also investigated. The porosity is defined as the Ag volumetric fraction before this process¹⁵. Figure 7 a) shows the time resolved reflectivity responses. While the oscillations last for several ns for the alloy NWs, they're mostly shorter than 1 ns in the case of the porous wires. This results in a much smaller quality factor for the first breathing mode, as it is shown on figure 7 b), which happen to be the only detected component. Nevertheless, a clear shift to lower frequencies after dealloying is observed, signature of a large decrease of the stiffness in such granular medium.

We have shown that pump-probe investigations with very high spectral resolution can be performed to detect breathing modes of Au-Ag alloy NWs with different gold molar fraction. Taking advantage of the suppression of the mechanical coupling between the substrates and the NWs, which are free-standing over trenches, several orders of EMs up to more than 46 GHz can be distinguished with high quality factors. Using the Pochhammer-Chree approach, both longitudinal and transverse velocities can be determine for the different molar fractions. The latter is rarely addressed in literature. The detection of an additional mode at lower frequency also allow to increase the accuracy of the transverse velocity determination using finite element approach. Similar investigation has been realized on porous Au NWs. This method paves the way to the elasticity evaluation in alloy and more importantly in porous single NWs.

ACKNOWLEDGMENTS

The employed NWs are part of the experiment UMAT, which was performed at the beam line X0 at the GSI Helmholtzzentrum fuer Schwerionenforschung, Darmstadt (Germany) in the frame of FAIR Phase-0.

- ¹L. Piraux, J. M. George, J. F. Despres, C. Leroy, E. Ferain, R. Legras, K. Ounadjela, and A. Fert, *Appl. Phys. Lett.* **65**, 2484 (1994).
- ²J. J. Mock, S. J. Oldenburg, D. R. Smith, D. A. Schultz, and S. Schultz, *Nano Lett.* **2**, 465 (2002).
- ³D. Zhang, Z. Liu, S. Han, C. Li, B. Lei, M. P. Stewart, J. Tour, and C. Zhou, *Nano Lett.* **4**, 2151 (2004).
- ⁴L. Piraux, S. Dubois, A. Fert, and L. Belliard, *The European Physical Journal B-Condensed Matter and Complex Systems* **4**, 413 (1998).
- ⁵Y. T. Chong, D. Görlitz, S. Martens, M. Y. E. Yau, S. Allende, J. Bachmann, and K. Nielsch, *Adv. Mater.* **22**, 2435 (2010).
- ⁶Y. Ding, M. Chen, and J. Erlebacher, *J. Am. Chem. Soc.* **126** (2004).
- ⁷X. Zhang and Y. Ding, *Catal. Sci. Technol.* **3**, 2862 (2013).
- ⁸E. D. Herderick, J. S. Tresback, A. L. Vasiliev, and N. P. Padture, *Nanotechnology* **18**, 155204 (2007).
- ⁹L. J. Lauhon, M. S. Gudiksen, D. Wang, and C. M. Lieber, *Nature* **420**, 57 (2002).
- ¹⁰M. Cassinelli, S. Müller, K. O. Voss, C. Trautmann, F. Völkein, J. Gooth, K. Nielsch, and M. E. Toimil-Molares, *Nanoscale* **9**, 3169 (2017).
- ¹¹J. Zhu, *Nanoscale Res. Lett.* **4**, 977 (2009).
- ¹²J. Goldberger, R. He, Y. Zhang, S. Lee, H. Yan, H. J. Choi, and P. Yang, *Nature* **422**, 599 (2003).
- ¹³C. D. Keating and M. J. Natan, *Adv. Mater.* **15**, 451 (2003).
- ¹⁴S. R. Nicewarner-Peña, A. J. Carado, K. E. Shale, and C. D. Keating, *J. Phys. Chem. B.* **107**, 7360 (2003).
- ¹⁵I. Schubert, C. Huck, P. Kröber, F. Neubrech, A. Pucci, M. E. Toimil-Molares, C. Trautmann, and J. Vogt, *Adv. Opt. Mater.* **4**, 1838 (2016).
- ¹⁶S. O. Kucheyev, J. R. Hayes, J. Biener, T. Huser, C. E. Talley, and A. V. Hamza, *Appl. Phys. Lett.* **89**, 053102 (2006).
- ¹⁷R. Zeis, A. Mathur, G. Fritz, J. Lee, and J. Erlebacher, *J. Power Sources* **165**, 65 (2007).
- ¹⁸M. Law, L. E. Greene, A. Radenovic, T. Kuykendall, J. Liphardt, and P. Yang, *J. Phys. Chem. B.* **110**, 22652 (2006).
- ¹⁹L. E. Greene, M. Law, B. D. Yuh, and P. Yang, *J. Phys. Chem. C.* **111**, 18451 (2007).
- ²⁰J. A. Czaban, D. A. Thompson, and R. R. LaPierre, *Nano Lett.* **9**, 148 (2008).
- ²¹D. Kramer, R. N. Viswanath, and J. Weissmüller, *Nano Lett.* **4**, 793 (2004).
- ²²C. Jean, L. Belliard, T. W. Cornelius, O. Thomas, Y. Pennec, M. Cassinelli, M. E. Toimil-Molares, and B. Perrin, *Nano Lett.* **16**, 6592 (2016).
- ²³F. Xu, Y. Guillet, S. Ravaine, and B. Audoin, *Phys. Rev. B* **97**, 165412 (2018).
- ²⁴N. Mingo, L. Yang, D. Li, and A. Majumdar, *Nano Lett.* **3**, 1713 (2003).
- ²⁵A. Boukai, Y. Bunimovich, J. Tahir-Kheli, J.-K. Yu, W. A. G. III, and J. R. Heath, *Nature* **451**, 168 (2008).
- ²⁶N. Bannov, V. Aristov, V. Mitin, and M. A. Stroschio, *Phys. Rev. B* **51**, 9930 (1995).
- ²⁷D. Li, Y. Wu, P. Kim, L. Shi, P. Yang, and A. Majumdar, *Appl. Phys. Lett.* **83**, 2934 (2003).
- ²⁸A. I. Hochbaum, R. Chen, R. D. Delgado, W. Liang, E. C. Garnett, M. Najarian, A. Majumdar, and P. Yang, *Nature* **451**, 163 (2008).
- ²⁹J. Krieg, R. Giraud, H. Funke, J. Dufouleur, W. Escoffier, C. Trautmann, and M. E. Toimil-Molares, *Journal of Physics and Chemistry of Solid* **9**, 3169 (2017).
- ³⁰E. W. Wong, P. E. Sheehan, and C. M. Lieber, *Science* **277**, 1971 (1997).
- ³¹C. Y. Nam, P. Jaroenapibal, D. Tham, D. E. Luzzi, S. Evoy, and J. E. Fischer, *Nano Lett.* **6** (2006).
- ³²A. Crut, P. Maioli, N. Del Fatti, and F. Vallée, *Chem. Soc. Rev.* **43**, 3921 (2014).
- ³³M. A. van Dijk, M. Lippitz, and M. Orrit, *Phys. Rev. Lett.* **95**, 267406 (2005).
- ³⁴J. Burgin, P. Langot, N. Del Fatti, F. Vallée, W. Huang, and M. A. El-Sayed, *J. Phys. Chem. C* **112**, 11231 (2008).
- ³⁵R. Marty, A. Arbouet, C. Girard, A. Mlayah, V. Paillard, V. K. Lin, S. L. Teo, and S. Tripathy, *Nano Lett.* **11**, 3301 (2011).
- ³⁶T. A. Kelf, Y. Tanaka, O. Matsuda, E. M. Larsson, D. S. Sutherland, and O. B. Wright, *Nano Lett.* **11**, 3893 (2011).
- ³⁷H. Staleva and G. V. Hartland, *J. Phys. Chem. C* **112**, 7535 (2008).
- ³⁸P. Zijlstra, A. L. Tchepotareva, J. W. Chon, M. Gu, and M. Orrit, *Nano Lett.* **8**, 3493 (2008).
- ³⁹P. M. Jais, D. B. Murray, R. Merlin, and A. V. Bragas, *Nano Lett.* **11**, 3685 (2011).
- ⁴⁰V. Juvé, A. Crut, P. Maioli, M. Pellarin, M. Broyer, N. Del Fatti, and F. Vallée, *Nano Lett.* **10**, 1853 (2010).
- ⁴¹S. C. Yang, Y. C. Wu, P. A. Mante, C. C. Chen, H. P. Chen, H. Y. Chou, M. H. Shih, and C. K. Sun, *Appl. Phys. Lett.* **105**, 243101 (2014).
- ⁴²P. A. Mante, C. Y. Ho, L. W. Tu, and C. K. Sun, *Opt. Exp.* **20**, 18717 (2012).
- ⁴³P. A. Mante, Y. C. Wu, C. Y. Ho, and C. K. Sun, *Nano Lett.* **13**, 1139 (2013).
- ⁴⁴H. Staleva and G. V. Hartland, *Adv. Funct. Mater.* **18**, 3809 (2008).
- ⁴⁵T. A. Major, A. Crut, B. Gao, S. S. Lo, N. Del Fatti, F. Vallée, and G. V. Hartland, *Phys. Chem. Chem Phys* **15**, 4169 (2013).
- ⁴⁶L. Belliard, T. W. Cornelius, B. Perrin, N. Kacemi, L. Beccera, O. Thomas, M. E. Toimil-Molares, and M. J. Cassinelli, *J. Appl. Phys.* **114**, 193509 (2013).
- ⁴⁷T. Devkota, D. Chakraborty, K. Yu, G. Beane, J. E. Sader, and G. V. Hartland, *Phys. Chem. Chem Phys.* **20**, 17687 (2018).
- ⁴⁸A. G. N. Sofiah, M. Samykano, K. Kadirgama, R. V. Mohan, and N. A. C. Lah, *Applied Materials Today* **11**, 320 (2018).
- ⁴⁹D. K. Kehoe and S. A. M. ad Y. K. Gun'ko, *Nanoscale* **11**, 4328 (2019).
- ⁵⁰L. Burr, I. Schubert, W. Sigle, C. Trautmann, and M. E. Toimil-Molares, *J. Phys. Chem. C.* **119**, 2094920956 (2015).
- ⁵¹T. Bienville, J. F. Robillard, L. Belliard, I. Roch-Jeune, A. Devos, and B. Perrin, *Ultrasonics* **44**, e1289 (2006).
- ⁵²C. Jean, L. Belliard, L. Becerra, and B. Perrin, *Appl. Phys. Lett.* **107**, 193103 (2015).
- ⁵³L. Pochhammer and J. Reine, *Angew. Math.* **81**, 324 (1876).
- ⁵⁴C. Chree, *Trans. Cambridge Phil. Soc.* **14**, 250 (1889).
- ⁵⁵P. A. Mante, L. Belliard, and B. Perrin, *Nanophotonics* **7**, 1759 (2018).